

**First measurement of direct photoproduction of the  $a_2(1320)^0$  meson on the proton**

A. Celentano<sup>1</sup>, M. Battaglieri,<sup>2,1</sup> R. De Vita,<sup>1</sup> L. Marsicano,<sup>1</sup> V. Mathieu,<sup>3</sup> A. Pilloni,<sup>4,1</sup> A. Szczepaniak,<sup>5,6,7</sup> K. P. Adhikari,<sup>8</sup> S. Adhikari,<sup>9</sup> M. J. Amarian,<sup>8</sup> G. Angelini,<sup>10</sup> H. Atac,<sup>11</sup> L. Barion,<sup>12</sup> I. Bedlinskiy,<sup>13</sup> Fatiha Benmokhtar,<sup>14</sup> A. Bianconi,<sup>15,16</sup> A. S. Biselli,<sup>17</sup> F. Bossù,<sup>18</sup> S. Boiarinov,<sup>2</sup> W. J. Briscoe,<sup>10</sup> W. K. Brooks,<sup>19,2</sup> D. Bulumulla,<sup>8</sup> V. D. Burkert,<sup>2</sup> D. S. Carman,<sup>2</sup> J. C. Carvajal,<sup>9</sup> P. Chatagnon,<sup>20</sup> T. Chetry,<sup>21</sup> G. Ciullo,<sup>12,22</sup> L. Clark,<sup>23</sup> P. L. Cole,<sup>24,25</sup> M. Contalbrigo,<sup>12</sup> O. Cortes,<sup>10</sup> V. Crede,<sup>26</sup> R. Cruz-Torres,<sup>27</sup> A. D'Angelo,<sup>28,29</sup> N. Dashyan,<sup>30</sup> M. Defurne,<sup>18</sup> A. Deur,<sup>2</sup> S. Diehl,<sup>31</sup> C. Djalali,<sup>32,33</sup> M. Dugger,<sup>34</sup> R. Dupre,<sup>20</sup> H. Egiyan,<sup>2,35</sup> M. Ehrhart,<sup>36</sup> A. El Alaoui,<sup>19</sup> L. El Fassi,<sup>21,36</sup> L. Elouadrhiri,<sup>2</sup> P. Eugenio,<sup>26</sup> G. Fedotov,<sup>37,\*</sup> R. Fersch,<sup>38,39</sup> A. Filippi,<sup>40</sup> G. Gavalian,<sup>2,35</sup> N. Gevorgyan,<sup>30</sup> F. X. Girod,<sup>2,18</sup> D. I. Glazier,<sup>23</sup> W. Gohn,<sup>31</sup> E. Golovatch,<sup>37</sup> R. W. Gothe,<sup>33</sup> K. A. Griffioen,<sup>39</sup> M. Guidal,<sup>20</sup> K. Hafidi,<sup>36</sup> H. Hakobyan,<sup>19,30</sup> N. Harrison,<sup>2</sup> M. Hattawy,<sup>8</sup> F. Hauenstein,<sup>8</sup> T. B. Hayward,<sup>39</sup> D. Heddle,<sup>38,2</sup> K. Hicks,<sup>32</sup> A. Hobart,<sup>20</sup> M. Holtrop,<sup>35</sup> Y. Ilieva,<sup>33,10</sup> D. G. Ireland,<sup>23</sup> B. S. Ishkhanov,<sup>37</sup> E. L. Isupov,<sup>37</sup> D. Jenkins,<sup>41</sup> H. S. Jo,<sup>42</sup> K. Joo,<sup>31</sup> S. Joosten,<sup>36</sup> D. Keller,<sup>43,32</sup> M. Khachatryan,<sup>8</sup> A. Khanal,<sup>9</sup> M. Khandaker,<sup>44,†</sup> A. Kim,<sup>31</sup> C. W. Kim,<sup>10</sup> W. Kim,<sup>42</sup> F. J. Klein,<sup>45</sup> V. Kubarovsky,<sup>2</sup> L. Lanza,<sup>28</sup> M. Leali,<sup>15,16</sup> P. Lenisa,<sup>12,22</sup> K. Livingston,<sup>23</sup> V. Lucherini,<sup>46</sup> I. J. D. MacGregor,<sup>23</sup> D. Marchand,<sup>20</sup> N. Markov,<sup>2,31</sup> V. Mascagna,<sup>47,16,‡</sup> M. E. McCracken,<sup>48</sup> B. McKinnon,<sup>23</sup> Z.-E. Meziani,<sup>36</sup> M. Mirazita,<sup>46</sup> V. Mokeev,<sup>2</sup> A. Movsisyan,<sup>12</sup> E. Munevar,<sup>10,§</sup> C. Munoz Camacho,<sup>20</sup> P. Nadel-Turonski,<sup>2</sup> K. Neupane,<sup>33</sup> S. Niccolai,<sup>20</sup> G. Niculescu,<sup>49</sup> M. Osipenko,<sup>1</sup> A. I. Ostrovidov,<sup>26</sup> M. Paolone,<sup>11</sup> L. L. Pappalardo,<sup>12,22</sup> R. Paremuzyan,<sup>35</sup> E. Pasyuk,<sup>2</sup> W. Phelps,<sup>10</sup> O. Pogorelko,<sup>13</sup> J. W. Price,<sup>50</sup> Y. Prok,<sup>8,43</sup> M. Ripani,<sup>1</sup> J. Ritman,<sup>51</sup> A. Rizzo,<sup>28,29</sup> G. Rosner,<sup>23</sup> J. Rowley,<sup>32</sup> F. Sabatié,<sup>18</sup> C. Salgado,<sup>44</sup> A. Schmidt,<sup>10</sup> R. A. Schumacher,<sup>48</sup> U. Shrestha,<sup>32</sup> D. Sokan,<sup>23</sup> O. Soto,<sup>46</sup> N. Sparveris,<sup>11</sup> S. Stepanyan,<sup>2</sup> I. I. Strakovsky,<sup>10</sup> S. Strauch,<sup>33</sup> J. A. Tan,<sup>42</sup> N. Tyler,<sup>33</sup> M. Ungaro,<sup>2,31</sup> L. Venturilli,<sup>15,16</sup> H. Voskanyan,<sup>30</sup> E. Voutier,<sup>20</sup> D. Watts,<sup>52</sup> X. Wei,<sup>2</sup> M. H. Wood,<sup>53,33</sup> N. Zachariou,<sup>52</sup> J. Zhang,<sup>43</sup> and Z. W. Zhao<sup>54</sup>

(The CLAS Collaboration)

<sup>1</sup>INFN, Sezione di Genova, 16146 Genova, Italy<sup>2</sup>Thomas Jefferson National Accelerator Facility, Newport News, Virginia 23606, USA<sup>3</sup>Departamento de Física Teórica and IPARCOS, Universidad Complutense de Madrid, 28040 Madrid, Spain<sup>4</sup>European Centre for Theoretical Studies and Nuclear Physics (ECT\*) and Fondazione Bruno Kessler, Strada delle Tabarelle 286, Villazzano (Trento) I-38123, Italy<sup>5</sup>Department of Physics, Indiana University, Bloomington, Indiana 47405, USA<sup>6</sup>Center for Exploration of Energy and Matter, Indiana University, Bloomington, Indiana 47403, USA<sup>7</sup>Theory Center, Thomas Jefferson National Accelerator Facility, Newport News, Virginia 23606, USA<sup>8</sup>Old Dominion University, Norfolk, Virginia 23529, USA<sup>9</sup>Florida International University, Miami, Florida 33199, USA<sup>10</sup>The George Washington University, Washington, D.C. 20052, USA<sup>11</sup>Temple University, Philadelphia, Pennsylvania 19122, USA<sup>12</sup>INFN, Sezione di Ferrara, 44100 Ferrara, Italy<sup>13</sup>National Research Centre Kurchatov Institute-ITEP, Moscow 117259, Russia<sup>14</sup>Duquesne University, 600 Forbes Avenue, Pittsburgh, Pennsylvania 15282, USA<sup>15</sup>Università degli Studi di Brescia, 25123 Brescia, Italy<sup>16</sup>INFN, Sezione di Pavia, 27100 Pavia, Italy<sup>17</sup>Fairfield University, Fairfield, Connecticut 06824, USA<sup>18</sup>IRFU, CEA, Université Paris-Saclay, F-91191 Gif-sur-Yvette, France<sup>19</sup>Universidad Técnica Federico Santa María, Casilla 110-V Valparaíso, Chile<sup>20</sup>Université Paris-Saclay, CNRS/IN2P3, IJCLab, 91405 Orsay, France<sup>21</sup>Mississippi State University, Mississippi State, Mississippi 39762-5167, USA<sup>22</sup>Università di Ferrara, 44121 Ferrara, Italy<sup>23</sup>University of Glasgow, Glasgow G12 8QQ, United Kingdom<sup>24</sup>Lamar University, 4400 MLK Boulevard, P.O. Box 10009, Beaumont, Texas 77710, USA<sup>25</sup>Idaho State University, Pocatello, Idaho 83209, USA<sup>26</sup>Florida State University, Tallahassee, Florida 32306, USA<sup>27</sup>Massachusetts Institute of Technology, Cambridge, Massachusetts 02139-4307, USA

\*Current address: Ohio University, Athens, Ohio 45701, USA.

†Current address: Idaho State University, Pocatello, Idaho 83209, USA.

‡Current address: Università degli Studi di Brescia, 25123 Brescia, Italy.

§Current address: Thomas Jefferson National Accelerator Facility, Newport News, Virginia 23606, USA.

<sup>28</sup>*INFN, Sezione di Roma Tor Vergata, 00133 Rome, Italy*<sup>29</sup>*Universita' di Roma Tor Vergata, 00133 Rome Italy*<sup>30</sup>*Yerevan Physics Institute, 375036 Yerevan, Armenia*<sup>31</sup>*University of Connecticut, Storrs, Connecticut 06269, USA*<sup>32</sup>*Ohio University, Athens, Ohio 45701, USA*<sup>33</sup>*University of South Carolina, Columbia, South Carolina 29208, USA*<sup>34</sup>*Arizona State University, Tempe, Arizona 85287-1504, USA*<sup>35</sup>*University of New Hampshire, Durham, New Hampshire 03824-3568, USA*<sup>36</sup>*Argonne National Laboratory, Argonne, Illinois 60439, USA*<sup>37</sup>*Skobeltsyn Institute of Nuclear Physics, Lomonosov Moscow State University, 119234 Moscow, Russia*<sup>38</sup>*Christopher Newport University, Newport News, Virginia 23606, USA*<sup>39</sup>*College of William and Mary, Williamsburg, Virginia 23187-8795, USA*<sup>40</sup>*INFN, Sezione di Torino, 10125 Torino, Italy*<sup>41</sup>*Virginia Tech, Blacksburg, Virginia 24061-0435, USA*<sup>42</sup>*Kyungpook National University, Daegu 41566, Republic of Korea*<sup>43</sup>*University of Virginia, Charlottesville, Virginia 22901, USA*<sup>44</sup>*Norfolk State University, Norfolk, Virginia 23504, USA*<sup>45</sup>*Catholic University of America, Washington, D.C. 20064, USA*<sup>46</sup>*INFN, Laboratori Nazionali di Frascati, 00044 Frascati, Italy*<sup>47</sup>*Università degli Studi dell'Insubria, 22100 Como, Italy*<sup>48</sup>*Carnegie Mellon University, Pittsburgh, Pennsylvania 15213, USA*<sup>49</sup>*James Madison University, Harrisonburg, Virginia 22807, USA*<sup>50</sup>*California State University, Dominguez Hills, Carson, California 90747, USA*<sup>51</sup>*Institute für Kernphysik (Juelich), Juelich, Germany*<sup>52</sup>*University of York, York YO10 5DD, United Kingdom*<sup>53</sup>*Canisius College, Buffalo, New York 14208, USA*<sup>54</sup>*Duke University, Durham, North Carolina 27708-0305, USA*

(Received 17 April 2020; revised 3 June 2020; accepted 31 August 2020; published 28 September 2020)

We present the first measurement of the reaction  $\gamma p \rightarrow a_2(1320)^0 p$  in the photon energy range 3.5–5.5 GeV and four-momentum transfer squared  $0.2 < -t < 2.0 \text{ GeV}^2$ . Data were collected with the CEBAF Large Acceptance Spectrometer detector at the Thomas Jefferson National Accelerator Facility. The  $a_2$  resonance was detected by measuring the reaction  $\gamma p \rightarrow \pi^0 \eta p$  and reconstructing the  $\pi^0 \eta$  invariant mass. The most prominent feature of the differential cross section is a dip at  $-t \approx 0.55 \text{ GeV}^2$ . This can be described in the framework of Regge phenomenology, where the exchange degeneracy hypothesis predicts a zero in the reaction amplitude for this value of the four-momentum transfer.

DOI: [10.1103/PhysRevC.102.032201](https://doi.org/10.1103/PhysRevC.102.032201)

It has been more than 40 yr since quantum chromodynamics was postulated as the theory of strong interactions. Although much progress has been made in understanding the high-energy phenomena through this theory, perturbative methods fail to describe the strong interaction at low energies. A clear understanding of this regime is of key importance since it corresponds to the dominant manifestation of the strong force in nature in terms of hadrons that constitute the bulk of the visible mass of the Universe.

Hadron spectroscopy is a valuable tool to investigate this regime. The measurement of the meson spectrum, searching for exotic states not compatible with the quark model, would provide access to the gluonic degrees of freedom that contribute to the quantum numbers of the hadrons. Investigating the properties and interactions of gluons is critical since their dynamics give rise to the strong interaction that binds the hadrons. In this context, the photoproduction of a  $\pi^0 \eta$  pair

on the proton ( $\gamma p \rightarrow \pi^0 \eta p$ ) is one of the most promising reaction channels since any  $P$ -wave resonance would be unambiguously interpreted as an *exotic* non- $q\bar{q}$  state. So far, only a few results have been reported for this reaction. At low energies, in the fully nonperturbative regime, high-quality cross-section data have been collected by the GRAAL [1], Crystal Ball, TAPS, A2 [2,3], and CB-ELSA [4,5] Collaborations. In the multi-GeV photon-beam energy range, optimal for meson spectroscopy, instead, no data have been published so far.

In this energy regime, the  $a_2(1320)$  meson is expected to make the dominant contribution to the  $\pi^0 \eta$  invariant-mass spectrum [6]. It can be, thus, taken as the reference state for a partial-wave analysis of this channel, for example, allowing for the interpretation of the variations of the  $P - D$  phase difference as a signature for the existence of exotic resonances [7,8]. Photoproduction of the charged  $a_2$  resonance has been

measured at the Stanford Linear Accelerator Center [9–11]. However, to the best of our knowledge, the neutral  $a_2$  channel has never been studied in photoproduction.

In this Rapid Communication, we report the first measurement of the neutral  $a_2(1320)$  meson photoproduction on the proton for photon-beam energies between 3.5 and 5.5 GeV, and four-momentum transferred squared ( $-t$ ) in the range of 0.2–2.0 GeV<sup>2</sup>. The differential cross-section  $d\sigma/dt$  was obtained by measuring the cross-section  $d^2\sigma/dt dM$  for the exclusive production of a  $\pi^0\eta$  pair on the proton, where  $M$  is the two-meson invariant mass and extracting the contribution of the  $a_2$  resonance in each kinematic bin. The measurement was performed with the CEBAF Large Acceptance Spectrometer (CLAS) in Hall B at the Jefferson Laboratory in a dedicated high-energy high-statistics run g12.

The experiment used a bremsstrahlung photon beam produced by the interaction of the primary  $E_0 = 5.72$ -GeV electron beam with a converter of  $10^{-4}$  radiation lengths. A magnetic spectrometer (photon tagger) with energy resolution  $0.1\%E_0$  was used to tag photons in the energy range of  $0.2E_0$ – $0.95E_0$  [12,13]. The target was a 40-cm-long cell filled with LH<sub>2</sub>. During the run, the high-intensity photon flux  $\approx 4 \times 10^7$   $\gamma$ /s was measured by sampling the “out-of-time” electron hits in the photon tagger [14].

Outgoing particles were measured with the CLAS detector [15]. This was a large-acceptance spectrometer, based on a toroidal magnet made of six superconducting coils arranged symmetrically around the beamline [16]. The momentum of a charged particle was determined from the radius of curvature of its trajectory in the magnetic field as measured by a multiwire drift-chamber system [17]. A set of plastic scintillator counters time of flight, installed behind the drift chambers, provided the time of flight of each particle [18]. Particle identification was performed through the  $\beta$  vs  $p$  technique. The energies and angles of the photons were measured with a lead and scintillator electromagnetic calorimeter, covering polar angles in the range  $8^\circ$ – $45^\circ$ , with energy resolution  $\sigma_E/E \approx 10\%/\sqrt{E(\text{GeV})}$ , and angular resolution  $\sigma_\theta \approx 10$  mrad [19].

The incoming photon was identified based on a  $\pm 1.0$ -ns coincidence between the vertex times obtained from the photon tagger and from the CLAS detector. The latter was determined by measuring the time of the outgoing charged particles with an array of plastic scintillator counters surrounding the target [20]. Due to the large photon flux, a fraction  $f_{\text{multi-}\gamma} = 12.5\%$  of events with more than one tagged photon within the coincidence window was observed. To avoid any bias in the analysis, these events were discarded. This effect was accounted for in the cross-section normalization by scaling the measured event yield by  $1/(1 - f_{\text{multi-}\gamma})$ . The systematic uncertainty of this correction, evaluated from the run-by-run variation of  $f_{\text{multi-}\gamma}$  is  $\approx 0.7\%$ .

The trigger condition required one charged particle and two photons in the CLAS detector. The corresponding efficiency was evaluated from minimum bias runs and found to be on average  $\varepsilon_{\text{trg}} = 80\%$ . A trigger efficiency map was derived and used to correct the cross-section normalization for the residual efficiency dependence on the charged particle impact point on the detector.

This analysis focuses on the  $\gamma p \rightarrow \pi^0\eta p$  reaction with all three final-state hadrons measured. Although the CLAS was optimized for charged multiparticle final states, this reaction could be measured thanks to the high statistics and the specific setup of the g12 run with the target moved upstream to maximize the detector acceptance. Events were selected requiring detection of both the proton and the four photons from the  $\pi^0$  and  $\eta$  decays. The standard g12 procedures, including momentum corrections and fiducial cuts, were applied [21]. A 4C kinematic fit (energy and momentum conservation imposed) was used to select events belonging to the exclusive  $\gamma p \rightarrow 4\gamma p$  reaction by introducing a cut on the corresponding confidence level (CL) [22,23]. To optimize this cut, the difference between the missing mass on the proton squared and the four photon invariant mass squared—here denoted as  $K$ —was considered. From energy and momentum conservation, it follows that signal events ( $\gamma p \rightarrow 4\gamma p$ ) are distributed around  $K = 0$  with a Gaussian distribution, whereas background events ( $\gamma p \rightarrow 4\gamma pX$ ) manifest as a tail in the  $K > 0$  region. Therefore, the following figure of merit (FOM) was defined

$$\text{FOM} = \frac{n_s}{\sqrt{n_s + n_b}}, \quad (1)$$

where  $n_s/2$  ( $n_s/2 + n_b$ ) was the number of events with  $K < 0$  ( $K > 0$ ). The optimal CL cut was determined by maximizing the FOM and found to be 1.86%.

The following procedure was then adopted to isolate the  $\gamma p \rightarrow \pi^0\eta p$  reaction. First, the photons were ordered event by event by naming  $\gamma_1$  and  $\gamma_2$  those with the smallest opening angle. This algorithm exploits the fact that due to the lower  $\pi^0$  mass, the two photons from its decay are expected to have, on average, a smaller opening angle than those from  $\eta$  decay. The corresponding efficiency, estimated from Monte Carlo simulations, is approximately 82% [24]. The correlation between the invariant masses of the two photon pairs  $M_{\gamma_1\gamma_2}$  vs  $M_{\gamma_3\gamma_4}$  is shown in Fig. 1. Signal events were identified as those corresponding to the bottom-right cluster centered at  $M_{\gamma_1\gamma_2} = M_{\pi^0}$ ,  $M_{\gamma_3\gamma_4} = M_\eta$ . A small fraction of events, corresponding to  $\approx 4\%$  of the main signal yield, appeared in the opposite combination and was not considered in the following.

After ordering the photons, the  $M_{\gamma_3\gamma_4}$  distribution showed a clear peak corresponding to  $\eta$  with some residual background events underneath. To reject these and extract the signal yield, the *sPlot* method was used [25]. This considers that events in the data sample originate from different independent sources and are characterized by a set of kinematic variables that can be split into two components. The method allows to reconstruct for each event source the distributions of *control variables* from the knowledge of the probability density function (PDF) associated with independent *discriminating variables*. In this analysis, the invariant mass  $M_{\gamma_3\gamma_4}$  was used discriminating variable, whereas  $M$  and  $M_{\gamma_1\gamma_2}$  were used as control variables. Two event sources were assumed: A signal source corresponding to the  $\eta$  meson decay, modeled with a Gaussian PDF with exponential tails, and a background source parametrized with a polynomial PDF. To avoid any



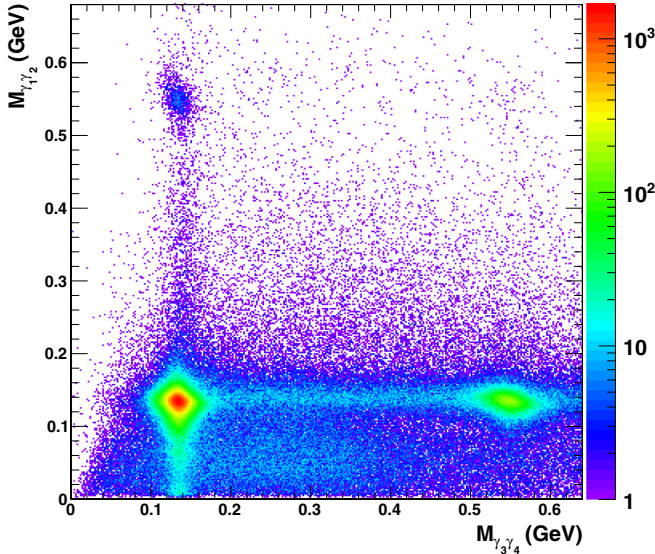


FIG. 1. Correlation between the invariant mass of the two photon pairs for exclusive  $\gamma p \rightarrow 4\gamma p$  events. In each event,  $\gamma_1$  and  $\gamma_2$  are the photons with the smallest opening angle. The bottom-right cluster contains signal events from the  $\gamma p \rightarrow \pi^0 \eta p$  reaction.

correlation between variables that was induced by the kinematic fit, resulting in a possible bias, events were first divided into independent  $M$  bins, and the  $sPlot$  analysis was applied independently in each of them. To assess the quality of the result, the  $M_{\gamma_1\gamma_2}$  distribution for the signal source was investigated, finding that no residual background was present below the  $\pi^0$  peak.

The CLAS acceptance and efficiency were evaluated by means of Monte Carlo simulations, based on a GEANT code that included knowledge of the full detector geometry and a realistic response to traversing particles. Since the extracted differential cross section is integrated over some of the independent kinematic variables, such as the  $\pi^0$  angles in the Gottfried-Jackson frame ( $\Omega_{GJ}$ ), the model used to generate Monte Carlo events had to be as close as possible to the real physical one. To this end,  $\gamma p \rightarrow \pi^0 \eta p$  events were first generated according to a bremsstrahlung photon-beam energy spectrum with a phase-space distribution and reconstructed

TABLE I. Summary of the systematic effects associated with the  $\gamma p \rightarrow p\pi^0\eta$  differential cross-section measurement. The effects marked as variable have a different contribution for each  $E_{\text{beam}}$ ,  $t$ , and  $M$  kinematic bin. The typical values are reported.

Systematic uncertainty source	Magnitude
Target properties	0.5%
Photon flux	5.7%
Beam photon selection	0.9%
Trigger efficiency	2.8%
$\eta \rightarrow \gamma\gamma$ branching fraction	0.5%
Kinematic fit	Variable, $\approx 3\%$
$sPlot$	Variable, $\approx 4\%$
Acceptance correction	Variable, $\approx 5\%$

through the same procedure used for real data. The result was used to compute the acceptance-corrected event distribution from which a new Monte Carlo sample was generated. The procedure was iterated until a good agreement between data and Monte Carlo was found for  $-t$  and for  $\Omega_{GJ}$  in each  $E_{\text{beam}}$  bin. In particular, the good matching between data and Monte Carlo for  $\Omega_{GJ}$  ensures that interference effects between different amplitudes contributing to the  $\pi^0\eta$  final state is properly considered when computing the detector acceptance. Finally, to account for the effect of the analysis procedures in the cross-section normalization, the same methods were applied to Monte Carlo events.

The differential cross-section  $d^2\sigma/dt dM$  is shown in Fig. 2 as a function of  $M$  for three photon-beam energy bins (rows) and five four-momentum transfer bins (columns). The error bars report the statistical uncertainty only. Table I summarizes the systematic uncertainties. The first four contributions are connected, respectively, to the uncertainty in the LH2 target properties (density and length), the absolute photon flux normalization, the trigger system efficiency, and the  $\eta \rightarrow \gamma\gamma$  branching fraction. The systematic uncertainties associated with the kinematic fit and the  $sPlot$  procedure have been evaluated by considering, in each bin, the relative variation of the cross section for different choices of the CL cut and of the degree of the background polynomial PDF. Finally, the systematic uncertainty on the CLAS acceptance was evaluated by varying the distribution used to generate the Monte Carlo events: A phase-space distribution was used, leading to a conservative estimate of this uncertainty contribution. The total systematic uncertainty was obtained by adding in quadrature all individual terms.

The differential cross-section  $d^2\sigma/dt dM$  shows two distinctive structures corresponding to the  $a_0(980)$  and  $a_2(1320)$  resonances. In particular, the  $a_2$  meson is clearly visible as a peak over a smooth background with the latter decreasing at higher beam energies. The exclusive  $a_2(1320)$  photoproduction cross-section  $d\sigma/dt$  has been extracted in the two largest photon-beam energy bins by modeling  $d^2\sigma/dt dM$  in the  $M$  range of 1.1–1.55 GeV as the incoherent sum of a resonance term and a smooth background, including contributions from both nonresonant  $\pi^0\eta$  photoproduction and from the residual high-mass tail of the  $a_0(980)$  state. The resonance term was written as the product of a  $(E_{\text{beam}}, -t)$ -dependent production coefficient and a Breit-Wigner function that describes the  $a_2$  line shape [26]. The background term was parametrized as a decreasing exponential function. The cross-section model was convoluted with the experimental  $M$  resolution, evaluated from Monte Carlo simulations. This ranged from a few MeV at high  $M$  values up to  $\approx 20$  MeV at  $M \approx 0.8$  GeV. A simultaneous  $\chi^2$  fit to all  $d^2\sigma/dt dM$  data points was then performed with a total of 28 free parameters (nine  $a_2$  production coefficients, nine background polynomial terms, nine background exponential slopes, and the  $a_2$  mass). In the Breit-Wigner formula, the  $a_2$  mass  $M_{a_2}$  was left to vary as a free parameter whereas the width  $\Gamma_{a_2}$  was fixed to the nominal PDG value of  $(113.4 \pm 1.3)$  MeV—the effect of this choice was studied and included in the systematic uncertainty. The  $\chi^2/\text{NDF}$  value was  $64.3/53 = 1.21$ , and the obtained  $M_{a_2}$  value was  $(1308 \pm 2)$  MeV, in very good agreement with the

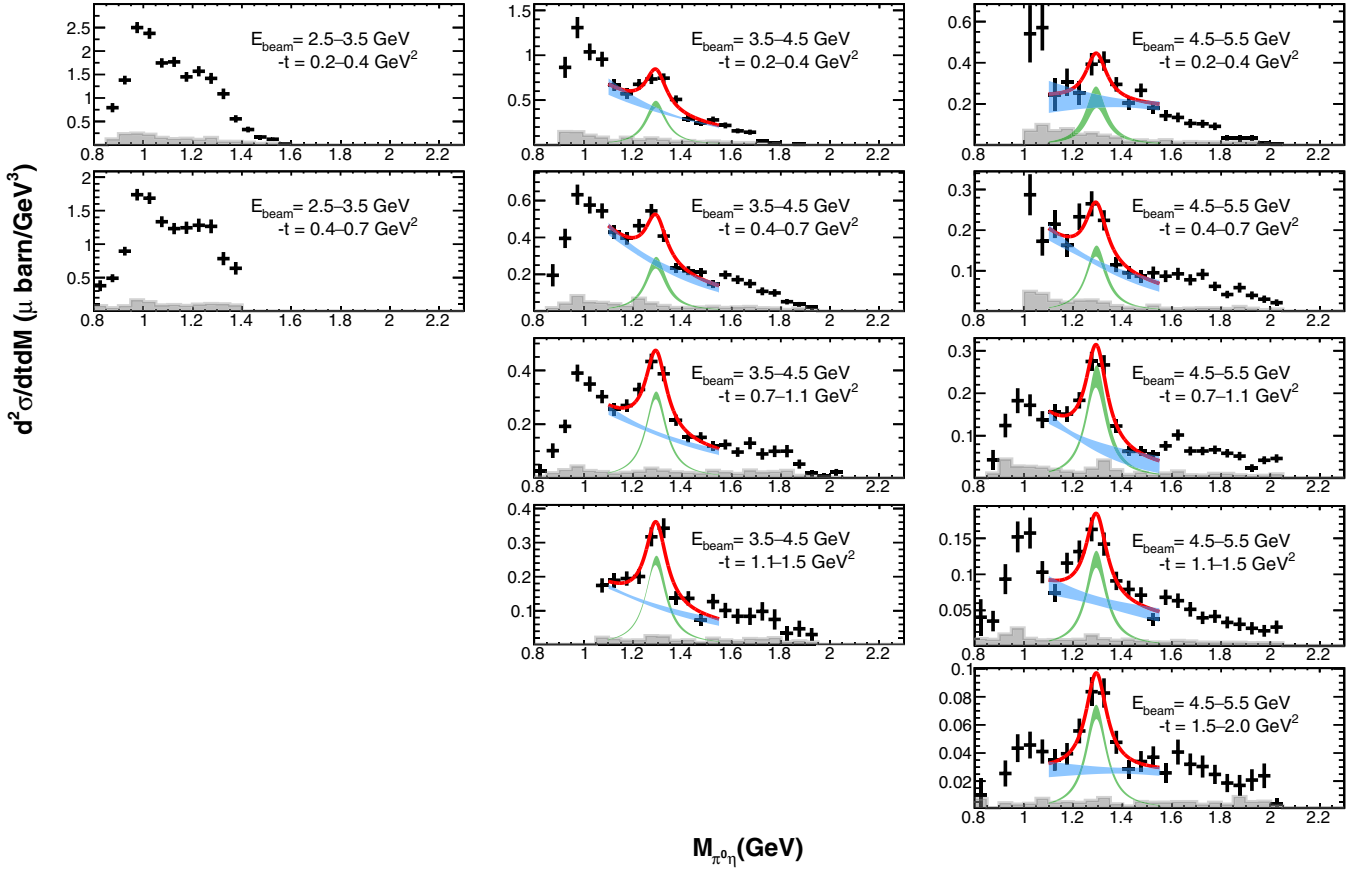


FIG. 2. Differential cross section for the reaction  $\gamma p \rightarrow \pi^0 \eta p$ . Each histogram reports the reaction differential cross-section  $d^2\sigma/dt dM$  as a function of the  $\pi^0 \eta$  invariant mass for the specific  $E_{\text{beam}}$  and  $-t$  bin reported in the same panel. The bottom gray-filled area in each panel shows the systematic uncertainty. The red curve is the result from the best fit performed with the model described in the text. The green and blue areas correspond, respectively, to the contribution of the  $a_2$  resonance and of the background, here, reported as the  $\pm 1\sigma$  systematic uncertainty bands around the central value. *These have been scaled vertically by a factor of  $\times 2$  for better readability.*

nominal PDG value of  $(1312.2 \pm 2.8)$  MeV. The fit result is reported for each kinematic bin in Fig. 2 as a red curve, whereas the green (blue) areas shows the  $a_2$  (background) contribution only, reported as the  $\pm 1\sigma$  systematic uncertainty band around the central value.

The differential cross section for the reaction  $\gamma p \rightarrow a_2(1320)^0 p$  was finally obtained by integrating the resonance term in each kinematic bin, accounting for the  $a_2 \rightarrow \pi^0 \eta$  branching fraction  $(14.5 \pm 1.2)\%$  [26]. The results are shown in Fig. 3 where the black (red) points refer to the photon energy range of 3.5–4.5 GeV (4.5–5.5 GeV). For each data point, the vertical bar shows the statistical uncertainty, evaluated from the covariance matrix of the  $\chi^2$  fit. The colored bands at the bottom show the systematic uncertainty, obtained summing quadratically the systematic uncertainty for  $d^2\sigma/dt dM$  and that associated with the fit procedure. This was evaluated by repeating the fit with different choices of the fit range and of the  $a_2$  width, that was varied within  $\pm 2\sigma$  around the nominal value.  $M_{\text{min}}$  ( $M_{\text{max}}$ ) was varied in the interval of 1.0–1.1 GeV (1.55–1.7 GeV). The nominal range reported previously corresponds to the fit with the smallest  $\chi^2/\text{NDF}$  value. The argument of the exponential function was

also replaced by polynomials of various orders. The systematic uncertainty was calculated, in each bin, as the rms of the cross-section values obtained from the different fits.

The most intriguing feature of the  $\gamma p \rightarrow a_2(1320)p$  cross section is the presence of a dip at  $-t_{\text{dip}} \approx 0.55$  GeV<sup>2</sup>, observed simultaneously at both beam energies. The hypothesis that this observed was just the effect of a statistical fluctuation was excluded at 99% CL as follows. We made a null hypothesis for  $d\sigma/dt$ , assuming a monotone shape: We tested both a linear and an exponential behavior. In particular, for this  $-t$  and  $E_{\text{beam}}$  range within the precision dictated by the large statistical errors, the latter functional form should generally provide a sufficient description of  $\frac{d\sigma}{dt}$  in the absence of a dip. We generated  $N = 10^5$  toy Monte Carlo datasets, resampling each measured  $d\sigma/dt$  point  $y_i \pm \sigma_i$  from a Gaussian distribution with  $\mu = y_i$  and  $\sigma = \sigma_i$ . Conservatively, we adopted, for  $\sigma_i$ , the quadratic sum of the statistical and systematic uncertainties, excluding the contributions that are independent from the kinematic bin. For each toy dataset and each beam energy, we performed a fit with the hypothesized functional form, excluding the point in the dip, extrapolating from it the expected cross-section value at  $-t_{\text{dip}}$ . The bin width was taken

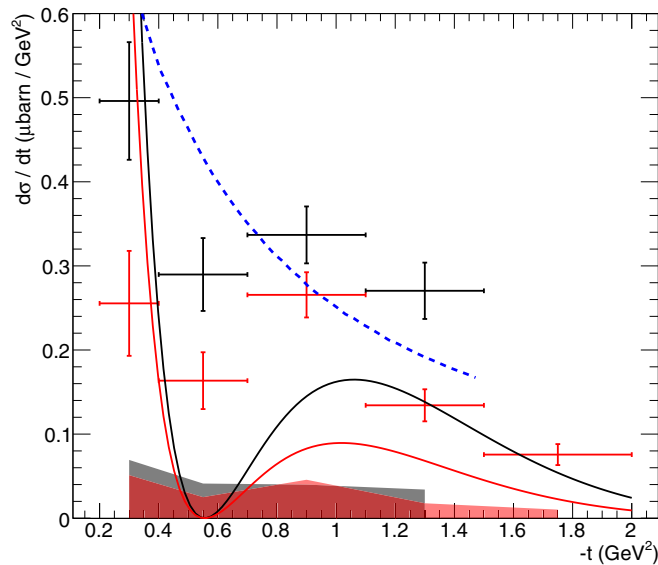


FIG. 3. Differential cross-section  $d\sigma/dt$  for the reaction  $\gamma p \rightarrow a_2(1320)p$  for  $E_{\text{beam}} = 3.5\text{--}4.5$  GeV (black) and  $E_{\text{beam}} = 4.5\text{--}5.5$  GeV (red). The vertical error bars show the statistical uncertainty, whereas horizontal error bars correspond to the  $-t$  bins width. The bottom bands show the systematic uncertainty. The continuous lines are predictions from the JPAC model [27], computed for a beam energy of 4 GeV (black) and 5 GeV (red), respectively. The blue dashed line is the prediction from the model by Xie *et al.* [28] for beam energy 3.4 GeV. For better readability, this was scaled vertically by a factor of  $\times 0.5$ .

into account by computing the latter as the average cross-section value inside the  $-t_{\text{dip}}$  bin. Finally, from the fraction of toy datasets in which both extrapolated values were lower than the toy dataset values at  $-t_{\text{dip}}$ , we computed the null hypothesis  $p$  value.

The origin of the dip and its specific location can be explained in the context of Regge theory [29]. In Fig. 3, we show the results of a model based on a Regge-theory production amplitude parametrization developed by the JPAC Collaboration [27], computed for the two beam energies 4 GeV (black) and 5 GeV (red). The amplitude includes the leading vector trajectories only, which have the  $\rho$  and  $\omega$  quantum numbers. Regge-resonance duality implies that the parameters of Regge amplitudes corresponding to these vector exchanges are closely related to the ones involving the tensor  $a_2$  and  $f_2$  mesons (exchange degeneracy hypothesis [29,30]). Since no scalar mesons lie on the  $a_2$  trajectory, the residue of the tensor exchange has to vanish when the Regge trajectory  $\alpha(t)$  is equal to zero to remove the scalar pole. Vector exchanges, which share the residues with the tensors, will, thus,

also vanish at  $\alpha(t) = 0$ , that is, at  $-t = m_{\rho,\omega}^2 \approx 0.55$  GeV<sup>2</sup>, leading to an exact zero in the cross section. However, sub-leading Regge poles or cut contributions can turn the zero of the amplitude into the dip observed in data and improve the description at higher  $-t$ . The results presented, here, are a pure prediction for  $d\sigma/dt$  since the model parameters were tuned on different datasets: The qualitative agreement between data and model, in particular, concerning the position of the dip, demonstrates the effectiveness of a reaction amplitude parametrization based on Regge phenomenology. The use of the present data to fine-tune the model parameters is beyond the scope of this work and will be the subject of a different publication [27]. Finally, we observe that our new data will help in understanding the nature of the  $a_2(1320)$  resonance. Although many authors describe it as a  $q\bar{q}$  state [31], others propose a different description. For example, Xie *et al.* [28] recently developed a model where  $a_2$  is a molecular state dynamically generated from the  $\rho - \omega$  and  $\rho - \phi$  interactions in the  $S$  wave with spin 2. This model predicts a smooth  $d\sigma/dt$  shape without any dip. Our data rule out this hypothesis.

To summarize, we have measured, for the first time, the reaction  $\gamma p \rightarrow \pi^0 \eta p$  in the photon-beam energy range of 3.5–5.5 GeV, and for four-momentum transferred squared values between 0.2 and 2.0 GeV<sup>2</sup>, extracting the cross section for the exclusive  $a_2(1320)$  photoproduction on the proton. The cross section shows a pronounced dip at  $-t \approx 0.55$  GeV<sup>2</sup>, which can be explained in the framework of Regge theory. Since the  $a_2(1320)^0$  is the most prominent structure present in the  $\pi^0 \eta$  invariant mass, detailed knowledge of its production cross section is valuable for any assessment of a possible exotic resonance contribution. This measurement will, thus, help high statistics photoproduction experiments, e.g., the CLAS12 [32], GLUEX [33], and BGOOD [34], to better understand the  $\pi^0 \eta$  mass spectrum and to properly describe the production of the dominant  $a_2$  resonance using it as a benchmark in the search for exotic states.

This work was supported by the U.S. Department of Energy (DOE), the U.S. National Science Foundation, the U.S. Jeffress Memorial Trust, the Physics and Astronomy Department, the Office of Research and Economic Development at Mississippi State University, the United Kingdom's Science and Technology Facilities Council (STFC), the Italian Istituto Nazionale di Fisica Nucleare; the French Institut National de Physique Nucléaire et de Physique des Particules, the French Centre National de la Recherche Scientifique, and the National Research Foundation of Korea. This material is based upon work supported by the U.S. Department of Energy, Office of Science, Office of Nuclear Physics under Contract No. DE-AC05-06OR23177. V.M. was supported by Comunidad Autónoma de Madrid through Programa de Atracción de Talento Investigador 2018 (Modalidad 1).

[1] J. Ajaka *et al.*, *Phys. Rev. Lett.* **100**, 052003 (2008).

[2] Crystal Ball, MAMI, TAPS, and A2 Collaborations, V. Kashevarov *et al.*, *Phys. Lett. B* **693**, 551 (2010).

[3] Crystal Ball, MAMI, TAPS, and A2 Collaborations, V. L. Kashevarov *et al.*, *Eur. Phys. J. A* **42**, 141 (2009).

- [4] CB-ELSA Collaboration, I. Horn *et al.*, *Phys. Rev. Lett.* **101**, 202002 (2008).
- [5] CB-ELSA Collaboration, I. Horn *et al.*, *Eur. Phys. J. A* **38**, 173 (2008), proceedings of the 12th international conference on hadron spectroscopy (Hadron 2007), Frascati, Italy, 2007.
- [6] COMPASS Collaboration, C. Adolph *et al.*, *Phys. Lett. B* **740**, 303 (2015).
- [7] JPAC Collaboration, A. Rodas *et al.*, *Phys. Rev. Lett.* **122**, 042002 (2019).
- [8] Crystal Barrel Collaboration, M. Albrecht *et al.*, *Eur. Phys. J. C* **80**, 453 (2020).
- [9] G. T. Condo, T. Handler, W. M. Bugg, G. R. Blackett, M. Pisharody, and K. A. Danyo, *Phys. Rev. D* **48**, 3045 (1993).
- [10] G. T. Condo *et al.*, *Phys. Rev. D* **41**, 3317 (1990).
- [11] J. Ballam, G. B. Chadwick, Z. G. T. Guiragossian, A. Levy, M. Menke, P. Seyboth, and G. E. Wolf, *Phys. Lett. B* **30**, 421 (1969).
- [12] D. I. Sober *et al.*, *Nucl. Instrum. Methods Phys. Res., Sect. A* **440**, 263 (2000).
- [13] S. Stepanyan, S. Boyarinov, H. Egiyan, L. Guo, D. Dale, M. Gabrielyan, L. Gan, A. Gasparian, A. Glamazdin, B. Mecking, I. Nakagawa, A. Teymurazyan, and M. Wood, *Nucl. Instrum. Methods Phys. Res., Sect. A* **572**, 654 (2007).
- [14] J. Ball and E. Pasyuk, Photon Flux Determination Through Sampling of “out-of-time” hits with the Hall B Photon Tagger, CLAS-NOTE 2005-002 (2005), [https://www.jlab.org/Hall-B/notes/clas\\_notes05/2005-002.pdf](https://www.jlab.org/Hall-B/notes/clas_notes05/2005-002.pdf).
- [15] B. A. Mecking *et al.*, *Nucl. Instrum. Methods Phys. Res., Sect. A* **503**, 513 (2003).
- [16] Y. A. Shishov, *Fiz. Elem. Chast. Atom. Yadra* **37**, 843 (2006) [*Phys. Part. Nucl.* **37**, 444 (2006)].
- [17] M. D. Mestayer *et al.*, *Nucl. Instrum. Methods Phys. Res., Sect. A* **449**, 81 (2000).
- [18] E. S. Smith *et al.*, *Nucl. Instrum. Methods Phys. Res., Sect. A* **432**, 265 (1999).
- [19] M. Amarian *et al.*, *Nucl. Instrum. Methods Phys. Res., Sect. A* **460**, 239 (2001).
- [20] Y. G. Sharabian, M. Battaglieri, V. Burkert, R. De Vita, L. Elouadrhiri, L. Guo, D. Kashy, V. Kubarovsky, G. Mutchler, M. Ostrick, M. Ripani, P. Rossi, A. Rottura, E. Pasyuk, and D. Weygand, *Nucl. Instrum. Methods Phys. Res., Sect. A* **556**, 246 (2006).
- [21] Z. Akbar *et al.*, g12Analysis Procedures, Statistics and Systematics, CLAS-NOTE 2017-002 (2017), <https://misportal.jlab.org/ul/Physics/Hall-B/clas/viewFile.cfm/2017-002.pdf?documentId=756>.
- [22] D. Keller, Techniques in kinematic fitting, CLAS-NOTE 2010-015 (2010), <https://misportal.jlab.org/ul/Physics/Hall-B/clas/viewFile.cfm/2010-015.pdf?documentId=614>.
- [23] M. Williams and C. A. Meyer, Kinematic Fitting in CLAS, CLAS-NOTE 2003-017 (2003), [https://www.jlab.org/Hall-B/notes/clas\\_notes03/03-017.pdf](https://www.jlab.org/Hall-B/notes/clas_notes03/03-017.pdf).
- [24] A. Celentano, The Forward Tagger detector for CLAS12 at Jefferson Laboratory and the MesonEx experiment, Ph.D. thesis, Università degli Studi di Genova, 2014.
- [25] M. Pivk and F. R. Le Diberder, *Nucl. Instrum. Methods Phys. Res., Sect. A* **555**, 356 (2005).
- [26] Particle Data Group, M. Tanabashi *et al.*, *Phys. Rev. D* **98**, 030001 (2018).
- [27] JPAC Collaboration, V. Mathieu, A. Pilloni, M. Albaladejo, L. Bibrzycki, A. Celentano, C. Fernandez-Ramirez, and A. P. Szczepaniak, *Phys. Rev. D* **102**, 014003 (2020).
- [28] J.-J. Xie, E. Oset, and L.-S. Geng, *Phys. Rev. C* **93**, 025202 (2016).
- [29] A. C. Irving and R. P. Worden, *Phys. Rep.* **34**, 117 (1977).
- [30] J. Mandula, J. Weyers, and G. Zweig, *Ann. Rev. Nucl. Part. Sci.* **20**, 289 (1970).
- [31] V. Cirigliano, A. Pich, G. Ecker, and H. Neufeld, *J. High Energy Phys.* **06** (2003) 012.
- [32] A. Celentano, *J. Phys.: Conf. Ser.* **424**, 012007 (2013).
- [33] GlueX Collaboration, A. Austregesilo, *Int. J. Mod. Phys.: Conf. Ser.* **46**, 1860029 (2018), proceedings of the 21st international conference on particles and nuclei (PANIC 17), Beijing, China, 2017.
- [34] BGO-OD Collaboration, S. Alef *et al.*, *Eur. Phys. J. A* **56**, 104 (2020).